

Adaptive Smoothing Spline for Trajectory Reconstruction

Zhanglong Cao¹, David Bryant¹, Tim Molteno², Colin Fox², and Matthew Parry¹

¹Department of Mathematics & Statistics, University of Otago, Dunedin 9016,
New Zealand

²Department of Physics, University of Otago, Dunedin 9016, New Zealand

Abstract

Trajectory reconstruction is the process of inferring the path of a moving object between successive observations. In this paper, we propose a smoothing spline – which we name the V-spline – that incorporates position and velocity information and a penalty term that controls acceleration. We introduce a particular adaptive V-spline designed to control the impact of irregularly sampled observations and noisy velocity measurements. A cross-validation scheme for estimating the V-spline parameters is given and we detail the performance of the V-spline on four particularly challenging test datasets. Finally, an application of the V-spline to vehicle trajectory reconstruction in two dimensions is given, in which the penalty term is allowed to further depend on known operational characteristics of the vehicle.

Keywords: trajectory reconstruction, smoothing spline, V-spline, cross-validation, adaptive penalty.

1 Introduction

Global Positioning System (GPS) devices are widely used to track vehicles and other moving objects. The devices generate a time series of noisy measurements of position and velocity that can then be used in batch and on-line reconstruction of trajectories.

GPS receivers are used to obtain trajectory information for a wide variety of reasons. The *TracMap* company, located in New Zealand and USA, produces GPS display units to aid precision farming in agriculture, horticulture and viticulture. With these units, operational data are collected and sent to a remote server for further analysis. GPS units also guide drivers of farm vehicles to locations on the farm that require specific attention.

Given a sequence of position vectors in a tracking system, the simplest way of constructing the complete trajectory of a moving object is by connecting positions with a sequence of lines, known as line-based trajectory representation (Agarwal et al., 2003). Vehicles with an omnidirectional drive or a differential drive can actually follow such a path in a drive-and-turn fashion, though it is highly inefficient (Gloderer and Hertle, 2010). This kind of non-smooth motion can cause slippage and over-actuation (Magid et al., 2006). By contrast, most vehicles typically follow smooth trajectories without sharp turns.

Several methods have been investigated to incorporate smoothness constraints into trajectory reconstruction. One approach uses the minimal length path that is continuously differentiable and consists of line segments or arcs of circles, with no more than three segments or arcs between successive positions (Dubins, 1957). This method is called Dubins curve and has been extended to other more complex vehicle models but is still limited to line segments and arcs of circles (Yang and Sukkarieh, 2010). However, there are still curvature discontinuities at the junctions between lines and arcs, leading to yaw angle errors (Wang et al., 2017).

Spline methods have been developed to construct smooth trajectories. Magid et al. (2006) propose a path-planning algorithm based on splines. The main objective of the method is the smoothness of the path, not a shortest or minimum-time path. Yu et al. (2004) give a piecewise cubic reconstruction found by matching the observed position and velocity at the endpoints of

each interval; this is essentially a Hermite spline. More generally, a B-spline gives a closed-form expression for the trajectory with continuous second derivatives and goes through the position points smoothly while ignoring outliers (Komoriya and Tanie, 1989; Ben-Arieh et al., 2004). B-splines are flexible and have minimal support with respect to a given degree, smoothness, and domain partition. Gasparetto and Zanotto (2007) use fifth-order B-splines to model the overall trajectory, allowing one to set kinematic constraints on the motion, expressed as the velocity, acceleration, and jerk. In the context of computer (or computerized) numerical control (CNC), Erkorkmaz and Altintas (2001) presented a quintic spline trajectory generation algorithm connecting a series of reference knots that produces continuous position, velocity, and acceleration profiles. Yang and Sukkarieh (2010) proposed an efficient and analytical continuous curvature path-smoothing algorithm based on parametric cubic Bézier curves that can fit sequentially ordered points.

A parametric approach only captures features contained in the preconceived class of functions (Yao et al., 2005) and increases model bias. To avoid this problem, nonparametric methods, such as smoothing splines, have been developed (Craven and Wahba, 1978). Let $\{t_i\}_{i=1}^n$ be a sequence of observation times in the interval $[a, b]$ satisfying $a \leq t_1 < t_2 < \dots < t_n \leq b$, and let $\mathbf{y} = \{y_1, \dots, y_n\}$ be the associated position observations. Smoothing spline estimates of $f(t)$ appear as a solution to the following minimization problem: find $\hat{f} \in \mathcal{C}^{(2)}[a, b]$ that minimizes the penalized residual sum of squares,

$$\text{RSS} = \sum_{i=1}^n (y_i - f(t_i))^2 + \lambda \int_a^b (f''(t))^2 dt \quad (1)$$

for a pre-specified value $\lambda > 0$ (Aydin and Tuzemen, 2012). In equation (1), the first term is a residual sum of squares and penalizes lack of fit. The second term is a roughness penalty term where the smoothing parameter λ varies from 0 to $+\infty$. (The roughness penalty term is a formalization of a mechanical device: if a thin piece of flexible wood, called a spline, is bent to the shape of the curve f , then the leading term in the strain energy is proportional to $\int f''(t)^2 dt$ (Green and Silverman, 1993).) The reconstruction cost, equation (1), is determined not only by its goodness-of-fit to the data quantified by the residual sum of squares but also by its roughness (Schwarz, 2000). For a given λ , minimizing equation (1) will give the best compromise between smoothness and goodness-of-fit. When $\lambda = 0$ the reconstruction is a smooth interpolation of the observation points; when $\lambda = \infty$ the reconstruction is a straight line. Notice that the first term in equation (1) depends only on the values of $f(t)$ at $t_i, i = 1, \dots, n$. Green and Silverman (1993) show that the function that minimizes the objective function for fixed values of $f(t_i)$ is a cubic spline: an interpolation of points via a continuous piecewise cubic function, with continuous first and second derivatives. The continuity requirements uniquely determine the interpolating spline, except at the boundaries (Sealfon et al., 2005).

Zhang et al. (2013) propose Hermite interpolation on each interval to fit position, velocity and acceleration with kinematic constraints. Their default trajectory formulation is a combination of several cubic splines on every interval or, alternatively, is a single function found by minimizing

$$p \sum_{i=1}^n |y_i - f(t_i)|^2 + (1 - p) \int_a^b |f''(t)|^2 dt, \quad (2)$$

where p is a smoothing parameter (Castro et al., 2006).

A conventional smoothing spline is controlled by one single parameter, which controls the smoothness of the spline on the whole domain. A natural extension is to allow the smoothing parameter to vary as a function of the independent variable, adapting to the change of roughness in different domains (Silverman, 1985; Donoho et al., 1995). The objective function is now of the form

$$\sum_{i=1}^n (y_i - f(t_i))^2 + \int_a^b \lambda(t) (f''(t))^2 dt. \quad (3)$$

Similar to the conventional smoothing spline problem, one has to choose the penalty function $\lambda(t)$. The fundamental idea of nonparametric smoothing is to let the data choose the amount

of smoothness, which consequently decides the model complexity (Gu, 1998). When λ is constant, most methods focus on data-driven criteria, such as cross-validation (CV), generalized cross-validation (GCV) (Craven and Wahba, 1978) and generalized maximum likelihood (GML) (Wahba, 1985). Allowing the smoothing parameter to be a function poses additional challenges, though Liu and Guo (2010) were able to extend GML to adaptive smoothing splines.

In this paper, we propose a smoothing spline – which we name the V-spline – that is obtained from noisy paired position data $\mathbf{y} = \{y_1, \dots, y_n\}$ and velocity data $\mathbf{v} = \{v_1, \dots, v_n\}$. In Section 2, the objective function for the V-spline is introduced that depends on velocity residuals $v_i - f'(t_i)$, as well as position residuals $y_i - f(t_i)$, and a parameter γ that controls the degree to which the velocity information is used in the reconstruction. We show that the V-spline can be written in terms of modified Hermite spline basis functions. We also introduce a particular adaptive V-spline that seeks to control the impact of irregularly sampled observations and noisy velocity measurements. A cross-validation scheme for estimating the V-spline parameters is given in section 3. Section 4 details the performance of the V-spline on simulated data based on the *Blocks*, *Bumps*, *HeaviSine* and *Doppler* test signals (Donoho and Johnstone, 1994). Finally, an application of the V-spline to a real 2-dimensional dataset is given in section 5.

2 The V-spline

We consider the situation of paired position data $\mathbf{y} = \{y_1, \dots, y_n\}$ and velocity data $\mathbf{v} = \{v_1, \dots, v_n\}$ at a sequence of times satisfying $a \leq t_1 < t_2 < \dots < t_n \leq b$. For $f \in \mathcal{C}_{\text{piecewise}}^{(2)}[a, b]$, we define the objective function

$$J[f] = \frac{1}{n} \sum_{i=1}^n (y_i - f(t_i))^2 + \frac{\gamma}{n} \sum_{i=1}^n (v_i - f'(t_i))^2 + \sum_{i=0}^n \lambda_i \int_{t_i}^{t_{i+1}} (f''(t))^2 dt, \quad (4)$$

where $t_0 := a$, $t_{n+1} := b$, $\gamma > 0$, and we have chosen the penalty function $\lambda(t)$ to be a piecewise constant function, i.e for $i = 0, \dots, n$,

$$\lambda(t) = \lambda_i, \quad t \in [t_i, t_{i+1}). \quad (5)$$

From now on, we will understand $\lambda(t)$ to be given by eq. (5) and we will often use λ to refer to the set of λ_i .

Theorem 1. *For $n \geq 2$, the objective function $J[f]$ is uniquely minimized by a cubic spline, piecewise on the intervals $[t_i, t_{i+1})$, $i = 1, \dots, n - 1$, and linear on $[a, t_1]$ and $[t_n, b]$.*

We term the minimizer of (4) the *V-spline* because it incorporates velocity information and because of its application to vehicle and vessel tracking. The proof of Theorem 1 is in Appendix B.

Remark: In the language of splines, the points t_1, \dots, t_n are the interior knots of the V-spline, and t_0, t_{n+1} are the exterior or boundary knots. Since the V-spline is linear on $[a, t_1]$ and $[t_n, b]$, without loss of generality we let $t_1 = a$ and $t_n = b$ from now on.

2.1 Constructing basis functions

It is convenient to construct basis functions from cubic Hermite splines (Hintzen et al., 2010). If y_0 and v_0 are the position and velocity at time 0, and y_1 and v_1 are the position and velocity at time 1, then for $s \in [0, 1]$, the cubic Hermite spline is defined as

$$f(s) = (2s^3 - 3s^2 + 1) y_0 + (s^3 - 2s^2 + s) v_0 + (-2s^3 + 3s^2) y_1 + (s^3 - s^2) v_1.$$

This implies that for an arbitrary interval $[t_i, t_{i+1})$, the relevant cubic spline basis functions are

$$h_{00}^{(i)}(t) = \begin{cases} 2 \left(\frac{t-t_i}{t_{i+1}-t_i} \right)^3 - 3 \left(\frac{t-t_i}{t_{i+1}-t_i} \right)^2 + 1 & t_i \leq t < t_{i+1} \\ 0 & \text{otherwise} \end{cases}, \quad (6)$$

$$h_{10}^{(i)}(t) = \begin{cases} \frac{(t-t_i)^3}{(t_{i+1}-t_i)^2} - 2 \frac{(t-t_i)^2}{t_{i+1}-t_i} + (t-t_i) & t_i \leq t < t_{i+1} \\ 0 & \text{otherwise} \end{cases}, \quad (7)$$

$$h_{01}^{(i)}(t) = \begin{cases} -2 \left(\frac{t-t_i}{t_{i+1}-t_i} \right)^3 + 3 \left(\frac{t-t_i}{t_{i+1}-t_i} \right)^2 & t_i \leq t < t_{i+1} \\ 0 & \text{otherwise} \end{cases}, \quad (8)$$

$$h_{11}^{(i)}(t) = \begin{cases} \frac{(t-t_i)^3}{(t_{i+1}-t_i)^2} - \frac{(t-t_i)^2}{t_{i+1}-t_i} & t_i \leq t < t_{i+1} \\ 0 & \text{otherwise} \end{cases}. \quad (9)$$

Consequently, the cubic Hermite spline $f^{(i)}(t)$ on an arbitrary interval $[t_i, t_{i+1})$ with two successive points $\{y_i, v_i\}$ and $\{y_{i+1}, v_{i+1}\}$ is expressed as

$$f^{(i)}(t) = h_{00}^{(i)}(t)y_i + h_{10}^{(i)}(t)v_i + h_{01}^{(i)}(t)y_{i+1} + h_{11}^{(i)}(t)v_{i+1}. \quad (10)$$

For V-splines, a slightly more convenient basis is given by $\{N_k(t)\}_{k=1}^{2n}$, where $N_1(t) = h_{00}^{(1)}(t)$, $N_2(t) = h_{10}^{(1)}(t)$, and for all $i = 1, 2, \dots, n-2$,

$$N_{2i+1}(t) = h_{01}^{(i)}(t) + h_{00}^{(i+1)}(t),$$

$$N_{2i+2}(t) = h_{11}^{(i)}(t) + h_{10}^{(i+1)}(t),$$

and

$$N_{2n-1}(t) = \begin{cases} h_{01}^{(n-1)}(t) & \text{if } t < t_n \\ 1 & \text{if } t = t_n \end{cases},$$

$$N_{2n}(t) = h_{11}^{(n-1)}(t).$$

Any $f \in \mathcal{C}_{\text{piecewise}}^{(2)}[a, b]$ can then be represented in the form

$$f(t) = \sum_{k=1}^{2n} N_k(t)\theta_k, \quad (11)$$

where $\{\theta_k\}_{k=1}^{2n}$ are parameters.

2.2 Computing the V-spline

In terms of the basis functions in the previous section, the objective function (4) is given by

$$nJ[f](\theta, \lambda, \gamma) = (\mathbf{y} - B\theta)^\top (\mathbf{y} - B\theta) + \gamma (\mathbf{v} - C\theta)^\top (\mathbf{v} - C\theta) + n\theta^\top \Omega_\lambda \theta, \quad (12)$$

where B and C are $n \times 2n$ matrices with components

$$[B]_{ij} = N_j(t_i) = \begin{cases} 1, & j = 2i - 1 \\ 0, & \text{otherwise} \end{cases} \quad (13)$$

$$[C]_{ij} = N_j'(t_i) = \begin{cases} 1, & j = 2i \\ 0, & \text{otherwise} \end{cases} \quad (14)$$

and Ω_λ is a $2n \times 2n$ matrix with components $[\Omega_\lambda]_{jk} = \int_a^b \lambda(t) N_j''(t) N_k''(t) dt$. In the following, we reserve the use of boldface for $n \times 1$ vectors and $n \times n$ matrices.

The detailed structure of Ω_λ is considered in Appendix A. It is convenient to write $\Omega_\lambda = \sum_{i=1}^{n-1} \lambda_i \Omega^{(i)}$, where $[\Omega^{(i)}]_{jk} = \int_{t_i}^{t_{i+1}} N_j''(t) N_k''(t) dt$. It is then evident that Ω_λ is a bandwidth four matrix.

Since equation (12) is a quadratic form in terms of θ , it is straightforward to establish that the objective function is minimized at

$$\hat{\theta} = (B^\top B + \gamma C^\top C + n\Omega_\lambda)^{-1} (B^\top \mathbf{y} + \gamma C^\top \mathbf{v}), \quad (15)$$

which can be identified as a generalized ridge regression. The fitted V-spline is then given by $\hat{f}(t) = \sum_{k=1}^{2n} N_k(t) \hat{\theta}_k$.

The V-spline is an example of a linear smoother (Hastie et al., 2009). This is because the estimated parameters in equation (15) are a linear combination of \mathbf{y} and \mathbf{v} . Denoting by $\hat{\mathbf{f}}$ and $\hat{\mathbf{f}}'$ the vector of fitted values $\hat{f}(t_i)$ and $\hat{f}'(t_i)$ at the training points t_i , we have

$$\hat{\mathbf{f}} = B (B^\top B + \gamma C^\top C + n\Omega_\lambda)^{-1} (B^\top \mathbf{y} + \gamma C^\top \mathbf{v}) =: \mathbf{S}_{\lambda,\gamma} \mathbf{y} + \gamma \mathbf{T}_{\lambda,\gamma} \mathbf{v} \quad (16)$$

$$\hat{\mathbf{f}}' = C (B^\top B + \gamma C^\top C + n\Omega_\lambda)^{-1} (B^\top \mathbf{y} + \gamma C^\top \mathbf{v}) =: \mathbf{U}_{\lambda,\gamma} \mathbf{y} + \gamma \mathbf{V}_{\lambda,\gamma} \mathbf{v} \quad (17)$$

where $\mathbf{S}_{\lambda,\gamma}$, $\mathbf{T}_{\lambda,\gamma}$, $\mathbf{U}_{\lambda,\gamma}$ and $\mathbf{V}_{\lambda,\gamma}$ are smoother matrices that depend only on t_i , $\lambda(t)$ and γ . It is not hard to show that $\mathbf{S}_{\lambda,\gamma}$ and $\mathbf{V}_{\lambda,\gamma}$ are symmetric, positive semidefinite matrices. Note that $\mathbf{T}_{\lambda,\gamma} = \mathbf{U}_{\lambda,\gamma}^\top$.

Theorem 2. *If $f(t)$ is a V-spline then, for almost all \mathbf{y} and \mathbf{v} , $f''(t)$ is continuous at the knots if and only if $\gamma = 0$ and $\lambda_i = \lambda_0$, for all $i = 1, \dots, n-1$.*

The proof of Theorem 2 is in Appendix C. The V-spline with $\gamma = 0$ and $\lambda_i = \lambda_0$ is simply the conventional smoothing spline.

2.3 The adaptive V-spline

Until now, we have not explicitly considered the impact of irregularly sampled observations or of noisy measurements of velocity on trajectory reconstruction. In order to do this, it is instructive to evaluate the contribution to the penalty term from the interval $[t_i, t_{i+1})$. Using (10), it is relatively straightforward to show that

$$f''(t) = \frac{1}{t_{i+1} - t_i} \left\{ 6 (\varepsilon_i^+ + \varepsilon_i^-) \frac{t - t_i}{t_{i+1} - t_i} - 2 (2\varepsilon_i^+ + \varepsilon_i^-) \right\}, \quad (18)$$

where $\varepsilon_i^+ = v_i - \bar{v}_i$, $\varepsilon_i^- = v_{i+1} - \bar{v}_i$ and $\bar{v}_i = (y_{i+1} - y_i)/(t_{i+1} - t_i)$ is the average velocity over the interval. The ε_i^\pm can be interpreted as the difference at time t_i and t_{i+1}^- respectively between the velocity implied by an interpolating Hermite spline and the velocity implied by a straight line reconstruction.

The contribution to the penalty term is then

$$4\lambda_i \frac{(\varepsilon_i^+)^2 + \varepsilon_i^+ \varepsilon_i^- + (\varepsilon_i^-)^2}{\Delta T_i}, \quad (19)$$

where $\Delta T_i = t_{i+1} - t_i$. We call the quantity $(\varepsilon_i^+)^2 + \varepsilon_i^+ \varepsilon_i^- + (\varepsilon_i^-)^2$, the square of the *discrepancy* of the velocity on the interval $[t_i, t_{i+1})$.

As a consequence of (19), larger time intervals will tend to contribute less to the penalty term (other things being equal). But this is exactly when we would expect the velocity at the endpoints of the interval to provide less useful information about the trajectory over the interval. In the case when the observed change in position is small, i.e. when $y_{i+1} - y_i = \bar{v}_i \Delta T_i \approx 0$, over-reliance on noisy measurements of velocity will result in “wiggly” reconstructions. In these two instances – graphically depicted in Figure 1a – we would like the V-spline to adapt and to favour straighter reconstructions; this is a deliberate design choice. We can achieve this by choosing

$$\lambda_i = \eta \frac{\Delta T_i}{\bar{v}_i^2}, \quad (20)$$

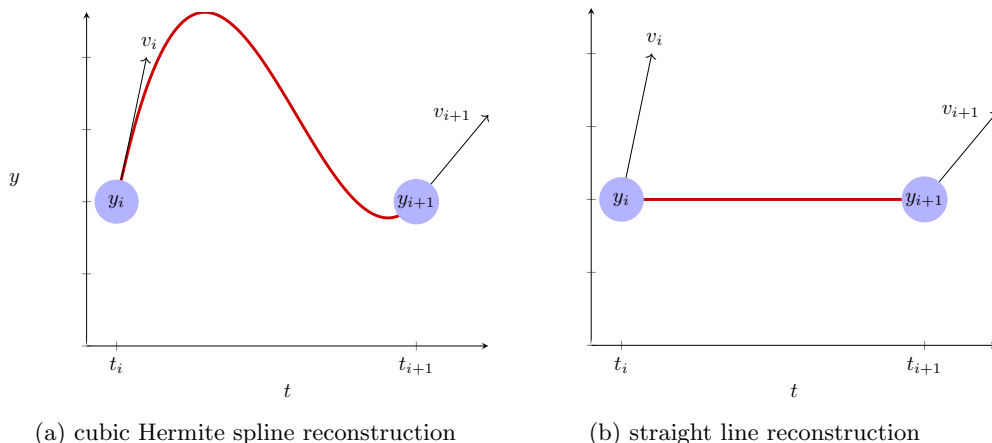


Figure 1: Comparing cubic Hermite spline reconstruction and straight line reconstruction. When $\Delta T_i = t_{i+1} - t_i$ is large or $\bar{v}_i \Delta T_i = y_{i+1} - y_i$ is small, the adaptive V-spline favours straighter reconstructions.

where η is a parameter to be estimated. The penalty term then takes a particularly compelling form: the contribution from the interval $[t_i, t_{i+1})$ (19) is proportional to

$$\left(\frac{\text{discrepancy in velocity}}{\text{average velocity}} \right)^2 \quad (21)$$

for all i . We call the resulting spline the *adaptive V-spline*. The spline when $\lambda_i = \lambda_0$, we call the *non-adaptive V-spline*.

3 Parameter selection and cross-validation

The issue of choosing the smoothing parameter is ubiquitous in curve estimation and there are two different philosophical approaches to the problem. The first is to regard the free choice of smoothing parameter as an advantageous feature of the procedure. The second is to let the data determine the parameter (Green and Silverman, 1993). We prefer the latter and use data to train our model and find the best parameters. The most well-known method for this is cross-validation.

In standard regression, which assumes the mean of the observation errors is zero, the true regression curve $f(t)$ has the property that if an observation y_i is omitted at time point t_i , the value $f(t_i)$ is the best predictor of y_i in terms of returning the least value of $(y_i - f(t_i))^2$. We use this observation to motivate a leave-one-out cross-validation scheme to estimate λ and γ for both the non-adaptive and the adaptive V-splines.

Let $\hat{f}^{(-i)}(t, \lambda, \gamma)$ be the minimizer of

$$\frac{1}{n} \sum_{j \neq i} (y_j - f(t_j))^2 + \frac{\gamma}{n} \sum_{j \neq i} (v_j - f'(t_j))^2 + \sum_{i=1}^{n-1} \lambda_i \int_{t_i}^{t_{i+1}} (f''(t))^2 dt, \quad (22)$$

and define the cross-validation score

$$\text{CV}(\lambda, \gamma) = \frac{1}{n} \sum_{i=1}^n \left(y_i - \hat{f}^{(-i)}(t_i, \lambda, \gamma) \right)^2. \quad (23)$$

We then choose λ and γ that jointly minimize $\text{CV}(\lambda, \gamma)$.

The following theorem establishes that we can compute the cross-validation score without knowing the $\hat{f}^{(-i)}(t, \lambda, \gamma)$:

Theorem 3. *The cross-validation score of a V-spline satisfies*

$$CV(\lambda, \gamma) = \frac{1}{n} \sum_{i=1}^n \left(\frac{y_i - \hat{f}(t_i) + \gamma \frac{T_{ii}}{1-\gamma V_{ii}} (v_i - \hat{f}'(t_i))}{1 - S_{ii} - \gamma \frac{T_{ii}}{1-\gamma V_{ii}} U_{ii}} \right)^2 \quad (24)$$

where \hat{f} is the V-spline smoother calculated from the full data set with smoothing parameter λ and γ , and $S_{ii} = [\mathbf{S}_{\lambda, \gamma}]_{ii}$, etc.

The proof of Theorem 3 is in Appendix D.

4 Simulation study

In this section, we give an extensive comparison of methods for regularly sampled time series data followed by simulation of irregularly sampled data. The comparison is based on the ability to reconstruct trajectories derived from *Blocks*, *Bumps*, *Heavisine* and *Doppler*, four functions which were used in (Donoho and Johnstone, 1994, 1995; Abramovich et al., 1998) to mimic problematic features in imaging, spectroscopy and other types of signal processing.

Letting $g(t)$ denote any one of *Blocks*, *Bumps*, *Heavisine* or *Doppler*, we treat $g(t)$ as the velocity of the trajectory $f(t)$, i.e. $f'(t) = g(t)$. Numerically, we calculate the position data via

$$f(t_{i+1}) = f(t_i) + \frac{g(t_i) + g(t_{i+1})}{2} (t_{i+1} - t_i), \quad (25)$$

where $f(t_1) = 0$. The observed position and velocity are then found by adding i.i.d. zero-mean Gaussian noise:

$$\begin{aligned} y_i &= f(t_i) + \varepsilon_i^{(f)}, \\ v_i &= g(t_i) + \varepsilon_i^{(g)}, \end{aligned} \quad (26)$$

where $\varepsilon_i^{(f)} \sim N(0, \sigma_f/SNR)$, $\varepsilon_i^{(g)} \sim N(0, \sigma_g/SNR)$, σ_f is the standard deviation of the positions $f(t_i)$, σ_g is the standard deviation of the velocities $g(t_i)$, and SNR is the signal-to-noise ratio, which we take to be 3 or 7.

4.1 Regularly sampled time series

We compare the performance of the adaptive V-spline with two wavelet transform reconstructions (Donoho and Johnstone, 1995; Abramovich et al., 1998), a spatially adaptive penalized spline known as the *P-spline* (Krivobokova et al., 2008; Ruppert et al., 2003), as well as the adaptive V-spline with $\gamma = 0$ and the non-adaptive V-spline. It is important to note that only the non-adaptive and adaptive V-splines incorporate velocity information. For the wavelet transform approach, we use both the *sure* threshold policy and *BayesThresh* with levels $l = 4, \dots, 9$. The V-spline parameters are obtained by minimizing the cross-validation score (24). Following Nason (2010), we fix $n = 1024$ in the simulations.

4.1.1 Numerical Examples

Figures 2 to 5 give reconstructions of the trajectories based on the *Blocks*, *Bumps*, *Heavisine* and *Doppler* functions respectively, when SNR= 7. Apart from the adaptive V-spline, we find all methods tend to oversmooth the reconstructions. Wavelet (*sure*) suffers from an occasional ‘‘high-frequency’’ breakdown and wavelet (*BayesThresh*) gives spurious fluctuations near the boundary knots. The *P-spline* gives a smoother reconstruction than wavelet reconstructions, but does not perform as well as the adaptive V-spline with $\gamma = 0$. The value of incorporating velocity information can be seen in the performance of the non-adaptive and adaptive V-splines. However, the non-adaptive V-spline can perform poorly when there are large absolute changes in velocity, e.g. in the *Blocks* and *Bumps* trajectories. Overall, the adaptive V-spline performs much better than the other methods and returns near-true reconstructions.

Figure 6 illustrates the trajectory velocities obtained by taking the first derivative of the adaptive V-spline trajectory. It is clear that the V-spline incorporates velocity information in order to improve trajectory reconstruction at the expense of smooth velocity reconstruction.

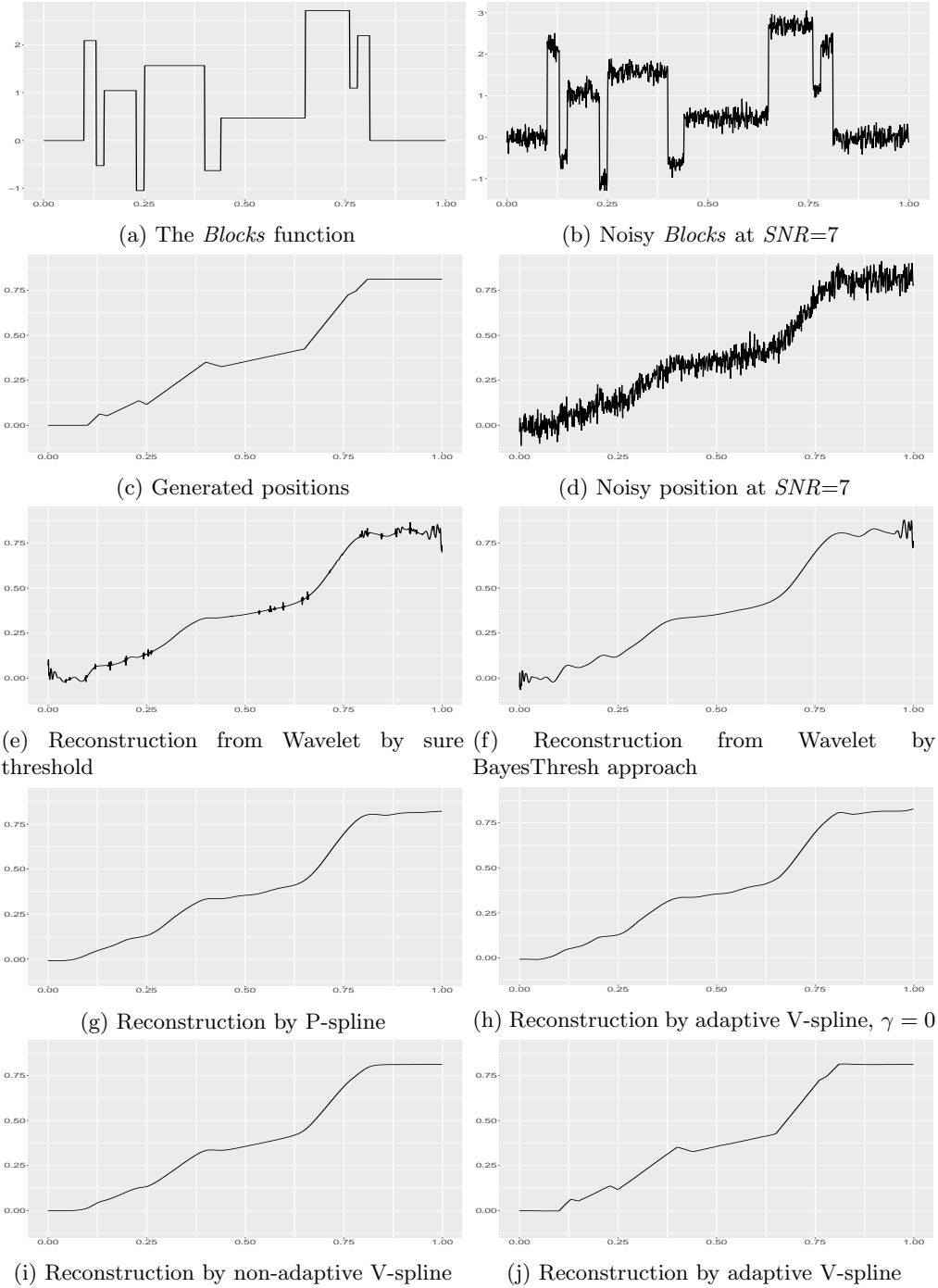


Figure 2: Numerical example: *Blocks*. Comparison of different reconstruction methods with simulated data.

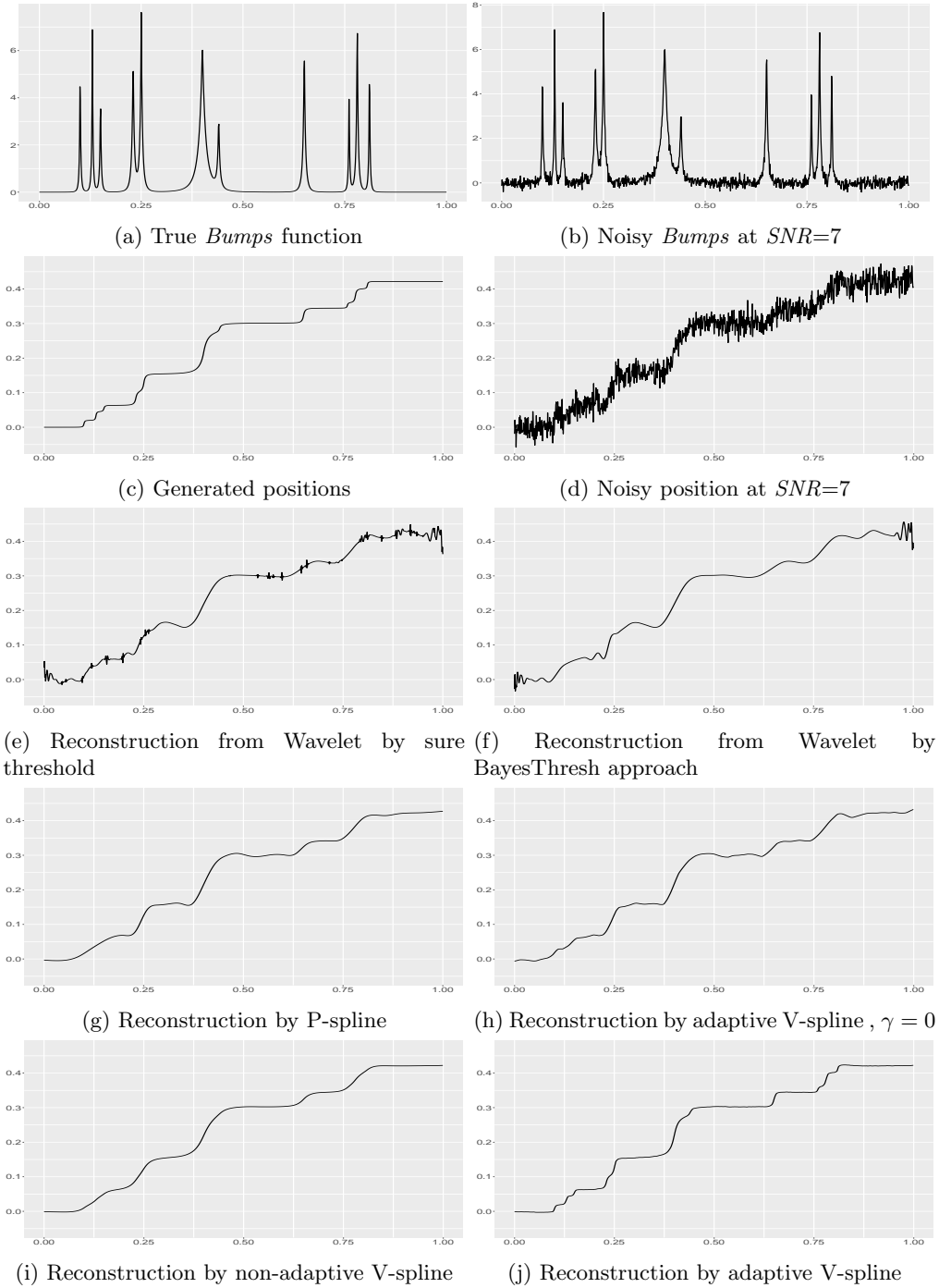


Figure 3: Numerical example: *Bumps*. Comparison of different reconstruction methods with simulated data.

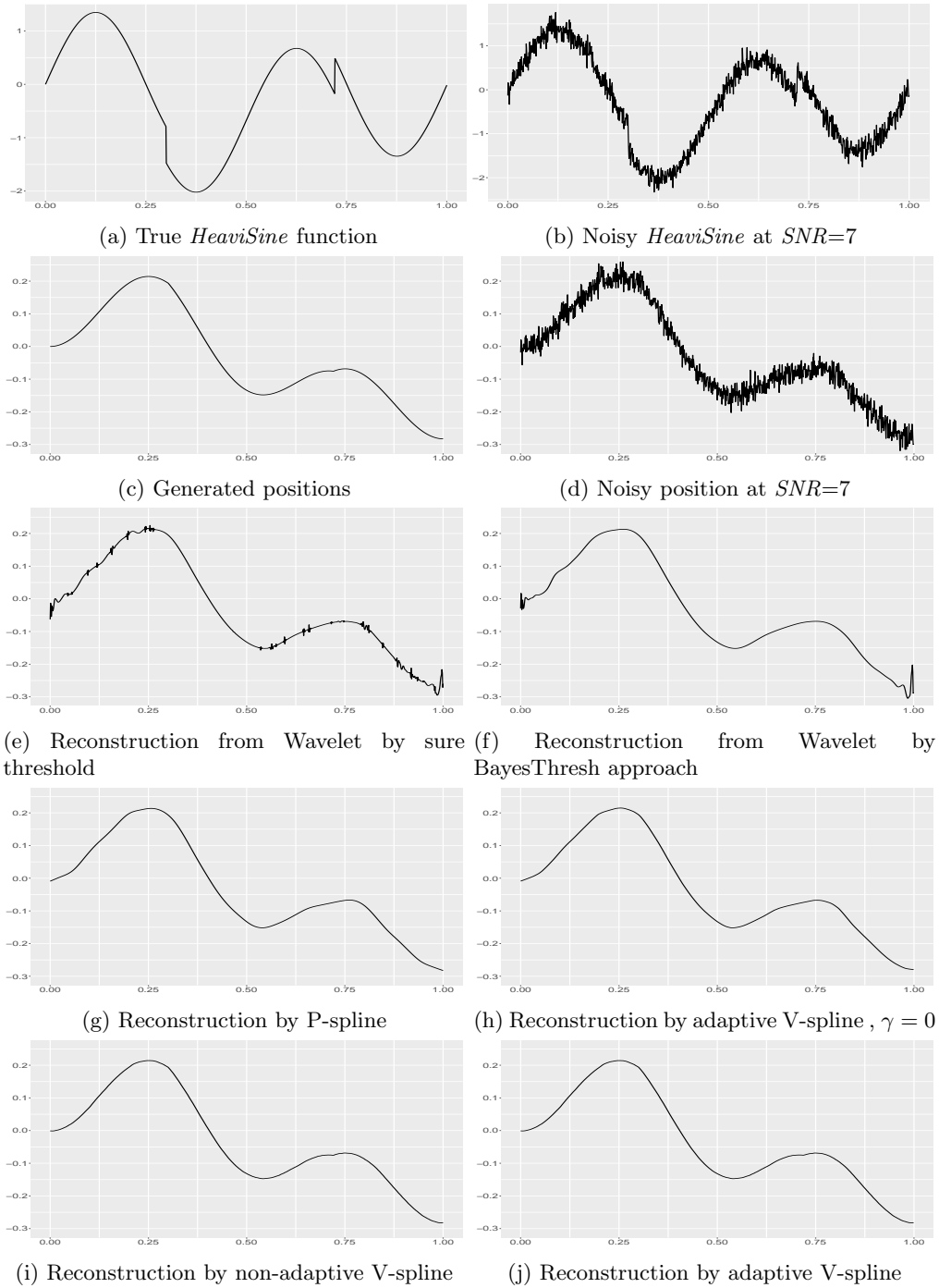


Figure 4: Numerical example: *HeaviSine*. Comparison of different reconstruction methods with simulated data.

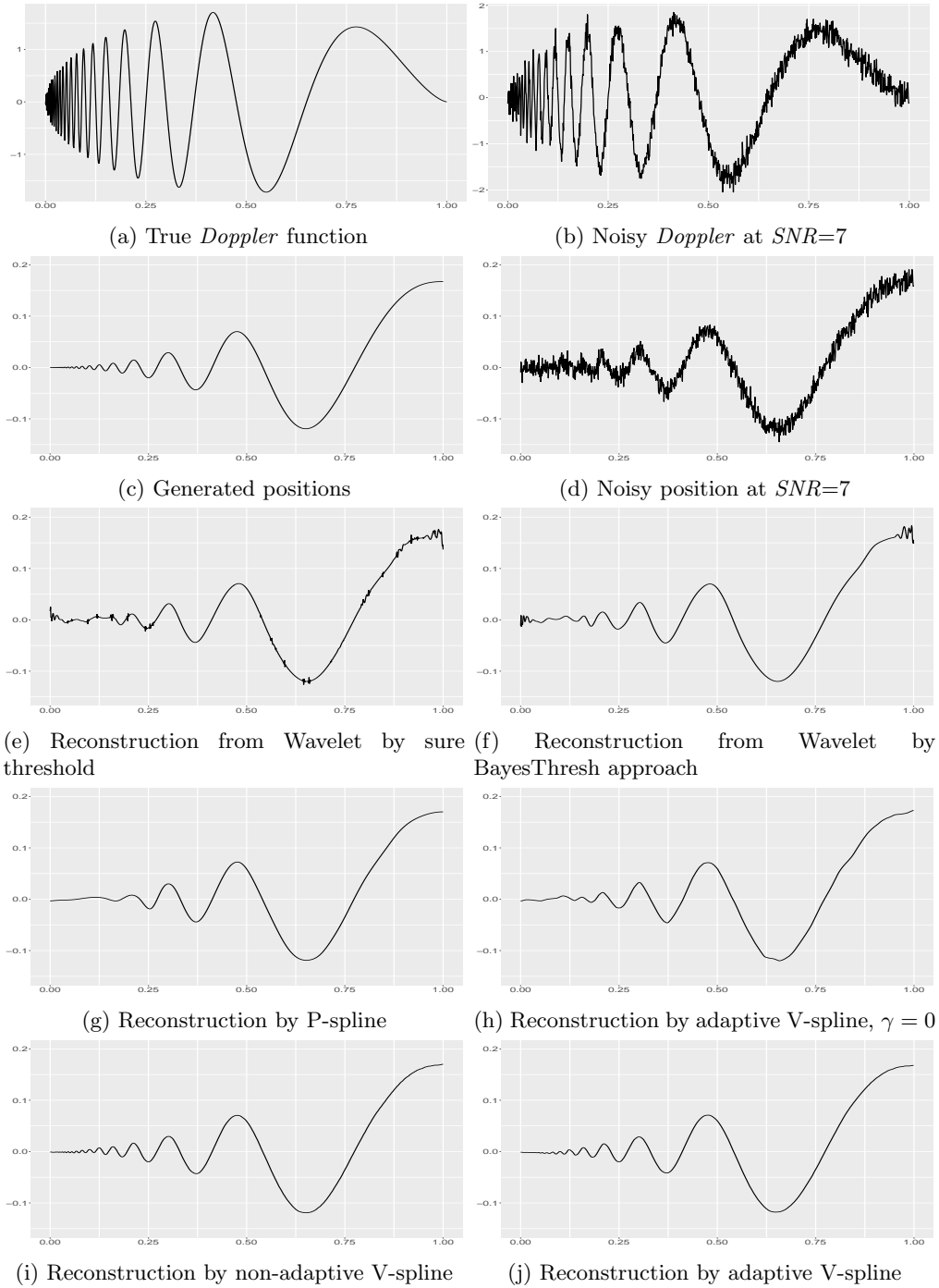


Figure 5: Numerical example: *Doppler*. Comparison of different reconstruction methods with simulated data.

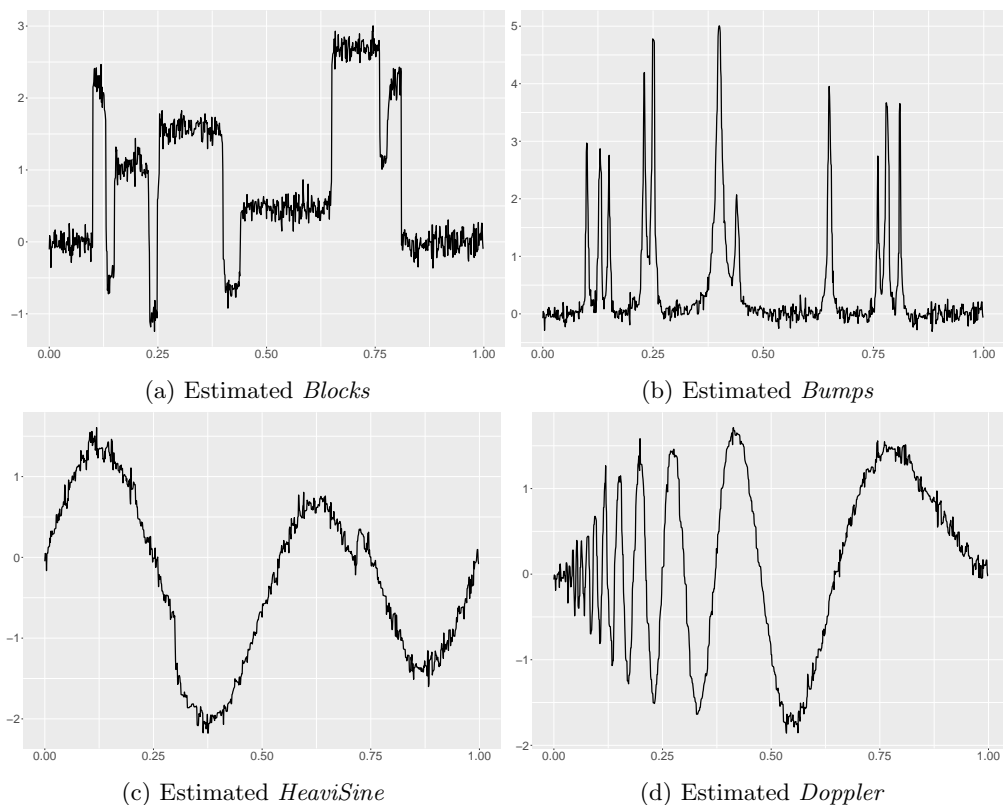


Figure 6: Trajectory velocities estimated by the adaptive V-spline.

4.1.2 Evaluation and residual analysis

To examine the performance of the adaptive V-spline, we compute the true mean squared error for each of the reconstructions:

$$\text{TMSE} = \frac{1}{n} \sum_{i=1}^n \left(f(t_i) - \hat{f}(t_i) \right)^2. \quad (27)$$

The results are shown in Table 1. The adaptive V-spline returns the smallest true mean squared errors for the *Blocks* and *Bumps* trajectories. For the *Heaviside* and *Doppler* trajectories, only the non-adaptive V-spline shows similar performance. Further analysis also shows that the residuals from the V-splines are not significantly correlated at any lag, as expected.

Table 2 shows the ability of the adaptive V-spline to retrieve the true SNR, calculated by

Table 1: True mean squared errors (TMSE) of different reconstruction methods. The numbers in bold indicate the least error in each scenario. VS_{λ_0} refers to the non-adaptive V-spline; $\text{VS}_{\gamma=0}$ refers to the adaptive V-spline with $\gamma = 0$; W refers to wavelet reconstruction.

| TMSE (10^{-6}) | SNR | V-spline | $\text{VS}_{\gamma=0}$ | VS_{λ_0} | P-spline | W(sure) | W(Bayes) |
|--------------------|-----|--------------|------------------------|-------------------------|----------|---------|----------|
| <i>Blocks</i> | 7 | 1.75 | 54.25 | 28.68 | 54.76 | 201.02 | 182.12 |
| | 3 | 16.44 | 152.5 | 30.76 | 171.59 | 1138.08 | 712.36 |
| <i>Bumps</i> | 7 | 1.64 | 23.44 | 21.10 | 24.21 | 71.71 | 69.26 |
| | 3 | 8.51 | 77.78 | 37.12 | 77.52 | 330.77 | 238.79 |
| <i>HeaviSine</i> | 7 | 1.53 | 7.80 | 1.56 | 9.54 | 55.37 | 44.88 |
| | 3 | 8.21 | 33.56 | 8.49 | 34.26 | 240.72 | 110.49 |
| <i>Doppler</i> | 7 | 1.51 | 6.67 | 1.08 | 8.26 | 14.87 | 12.01 |
| | 3 | 8.10 | 22.14 | 8.25 | 19.95 | 81.48 | 50.33 |

Table 2: Retrieved SNR.

| SNR | predefined value | generated f | V-spline \hat{f} |
|------------------|------------------|---------------|--------------------|
| <i>Blocks</i> | 7 | 6.9442 | 6.9485 |
| | 3 | 2.9761 | 2.9817 |
| <i>Bumps</i> | 7 | 6.9442 | 6.9548 |
| | 3 | 2.9761 | 2.9953 |
| <i>HeaviSine</i> | 7 | 6.9442 | 6.9207 |
| | 3 | 2.9761 | 2.9706 |
| <i>Doppler</i> | 7 | 6.9442 | 6.8757 |
| | 3 | 2.9761 | 2.9625 |

Table 3: TMSE of reconstructions from regularly and irregularly sampled data

| | TMSE $\times 10^{-6}$ | |
|------------------|-----------------------|-----------|
| | Regular | Irregular |
| <i>Blocks</i> | 3.5197 | 10.8596 |
| <i>Bumps</i> | 1.6662 | 6.2586 |
| <i>HeaviSine</i> | 1.1275 | 1.1077 |
| <i>Doppler</i> | 1.0101 | 1.7832 |

$$\sigma_{\hat{f}}/\sigma_{(\hat{f}-y)}.$$

4.2 Irregularly Sampled Time Series Data

In this section, we show that the proposed V-spline has the ability to reconstruct the true trajectory even though the data is irregularly sampled. For each of the functions of the previous section, we set SNR to 7 and generate a mother simulation of length $n = 1024$. We then obtain a regularly sampled daughter simulation of length 512 using the indices $1, 3, \dots, 1023$, and an irregularly sampled daughter simulation with 512 indices chosen at random.

Table 3 shows that the TMSE tends to increase when the data are irregularly sampled. In the case of *Blocks* and *Bumps*, the TMSE increases by a factor 3 or 4. However the ability to retrieve the true SNR does not appear to be affected; see Table 4.

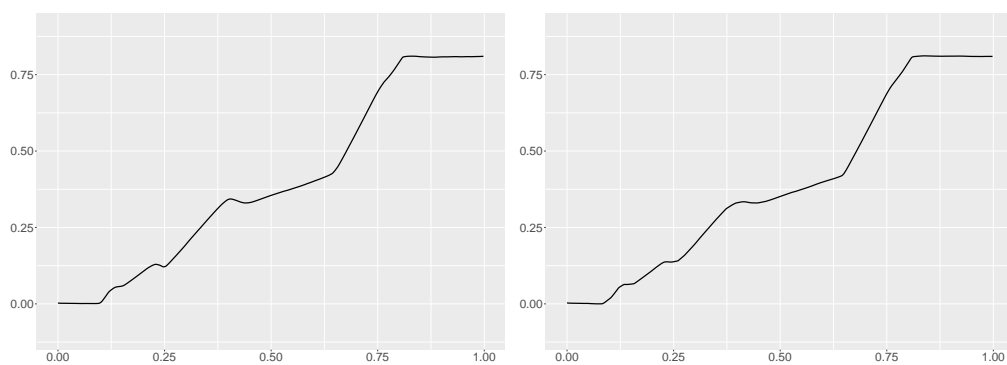
The reconstructions themselves are shown in Figure 7. In the irregularly sampled cases, the reconstruction tends to smooth some features in the underlying trajectories. In *Bumps* and, to a lesser extent, in *Doppler*, the reconstruction occasionally adds in features. This occurs when there are no sampled data at times when the underlying velocity is changing rapidly.

5 Inference of Tractor Trajectories

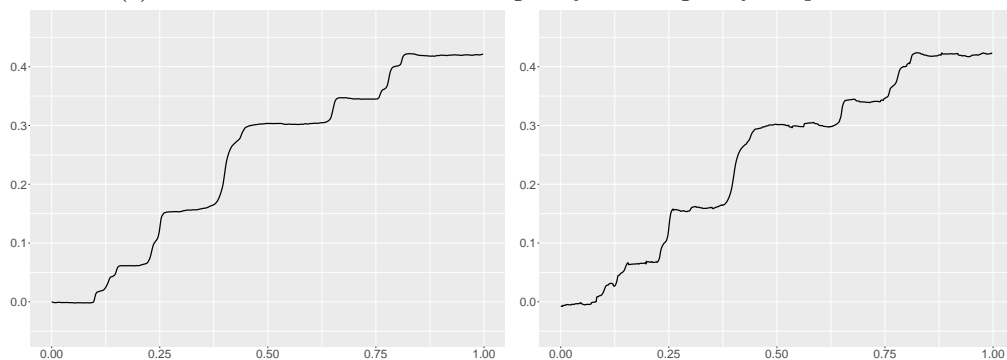
Real world vehicle trajectories exhibit many of the features seen in the test trajectories considered in the previous section, particularly the *Blocks*, *Bumps* and *HeaviSine* trajectories. In this section, we extend the V-spline to more than one dimension and apply it to a real dataset, which was obtained from a GPS unit mounted on a tractor working in a horticultural setting. The data was irregularly recorded with highly variable time differences ΔT_i . The original dataset contains $n = 928$ records of longitude, latitude, speed, bearing and the status of the tractor's

Table 4: Retrieved SNR of reconstructions from regularly and irregularly sampled data

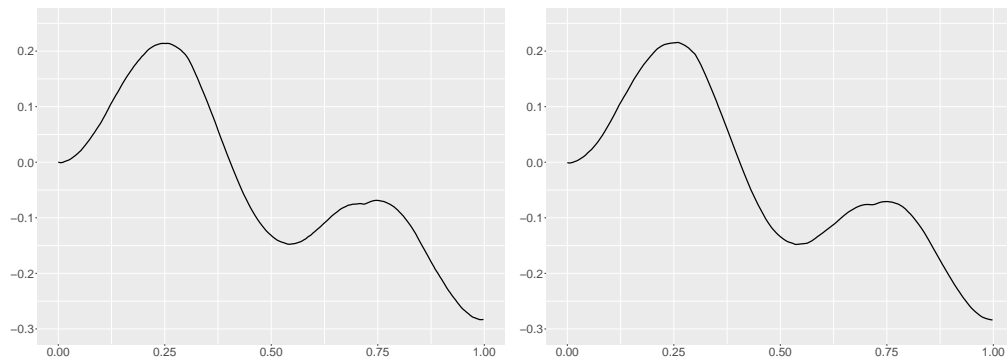
| SNR | Regular | Irregular |
|------------------|---------|-----------|
| <i>Blocks</i> | 7.0479 | 6.8692 |
| <i>Bumps</i> | 7.0241 | 7.1937 |
| <i>HeaviSine</i> | 7.2367 | 6.8793 |
| <i>Doppler</i> | 6.8692 | 7.3645 |



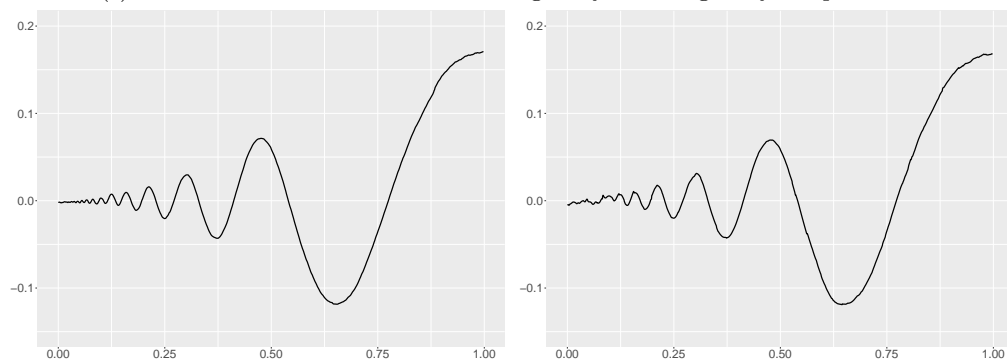
(a) Reconstruction of *Blocks* from regularly and irregularly sampled data



(b) Reconstruction of *Bumps* from regularly and irregularly sampled data



(c) Reconstruction of *HeaviSine* from regularly and irregularly sampled data



(d) Reconstruction of *Doppler* from regularly and irregularly sampled data

Figure 7: Comparison of adaptive V-spline trajectory reconstructions of regularly and irregularly sampled data.

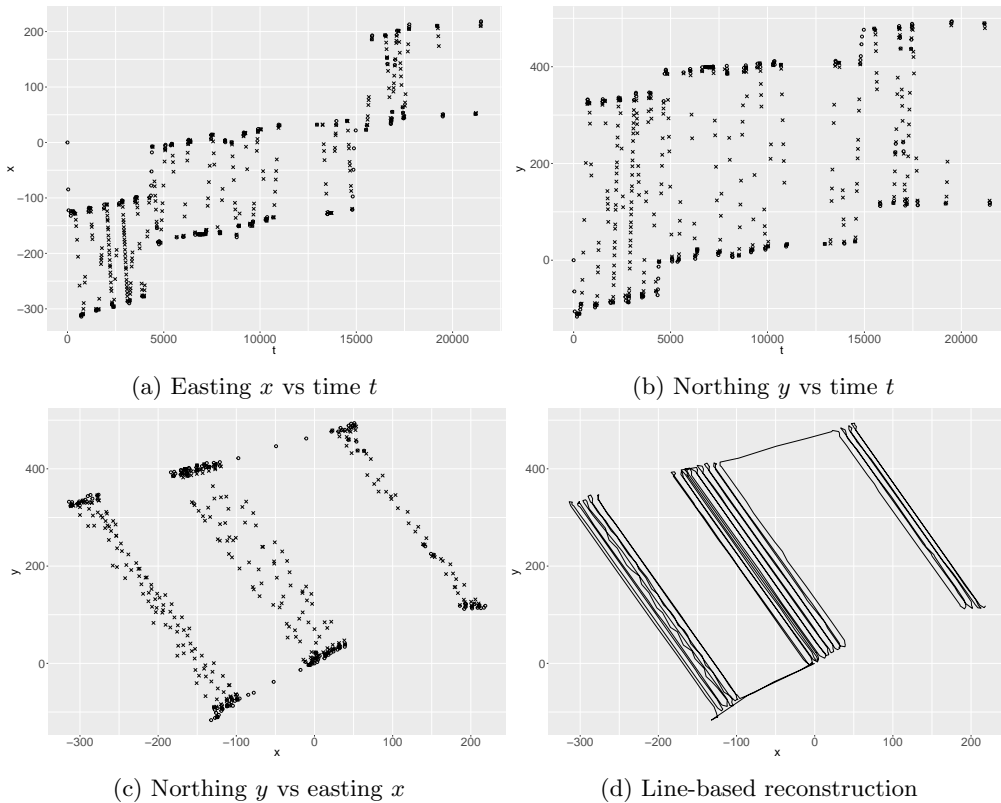


Figure 8: First 512 observations of position. Circles indicate the tractor boom is up; crosses indicate the boom is down. Figure 8d is the line-based reconstruction in which consecutive points are connected with straight lines.

boom sprayer. These data were converted into northing and easting, and the velocities in those directions. The boom status, “up” or “down”, denotes the operational state of the tractor, and may indicate different types of trajectories.

5.1 The V-spline in d -dimensions

To generalize the V-spline to d -dimensions, we consider the situation preceding eq. (4) but where now $y_i, v_i \in \mathbb{R}^d$. Then the function $f : [a, b] \rightarrow \mathbb{R}^d$ is a d -dimensional V-spline if it minimizes:

$$J[f] = \frac{1}{n} \sum_{i=1}^n \|y_i - f(t_i)\|_2^2 + \frac{\gamma}{n} \sum_{i=1}^n \|v_i - f'(t_i)\|_2^2 + \sum_{i=0}^n \lambda_i \int_{t_i}^{t_{i+1}} \|f''(t)\|_2^2 dt, \quad (28)$$

where $\|\cdot\|_2$ is the Euclidean norm in d -dimensions. For each direction $\alpha = 1, \dots, d$, the fitted V-spline has the form $\hat{f}^\alpha(t) = \sum_{k=1}^{2n} N_k(t) \hat{\theta}_k^\alpha$, where

$$\hat{\theta}^\alpha = (B^\top B + \gamma C^\top C + n\Omega_\lambda)^{-1} (B^\top \mathbf{y}^\alpha + \gamma C^\top \mathbf{v}^\alpha). \quad (29)$$

The parameters λ and γ are estimated by minimizing the cross-validation score:

$$CV(\lambda, \gamma) = \frac{1}{n} \sum_{i=1}^n \left\| \frac{y_i - \hat{f}(t_i) + \gamma \frac{T_{ii}}{1-\gamma V_{ii}} (v_i - \hat{f}'(t_i))}{1 - S_{ii} - \gamma \frac{T_{ii}}{1-\gamma V_{ii}} U_{ii}} \right\|_2^2 \quad (30)$$

In what follows, we allow the non-adaptive and adaptive V-splines to depend on the boom status. Specifically, letting $b_i = 0$ denote boom “up”, $b_i = 1$ denote boom “down”, and $\bar{v}_i =$

$\|y_{i+1} - y_i\|_2/\Delta T_i$ be the average velocity on the interval $[t_i, t_{i+1})$, the penalty term for the non-adaptive V-spline is

$$\lambda_i = b_i \lambda_d + (1 - b_i) \lambda_u, \quad (31)$$

and for the adaptive V-spline it is

$$\lambda_i = \{b_i \eta_d + (1 - b_i) \eta_u\} \frac{\Delta T_i}{\bar{v}_i^2}. \quad (32)$$

5.2 Trajectory reconstruction

It is instructive to first consider what happens when the northing and easting trajectories are reconstructed separately. To facilitate comparison with the wavelet approach we restrict attention to the first 512 observations. The data are shown in Figure 8. It is evident that the trajectory of the tractor is typically characterized by motion along rows with boom down, and tight turns at the ends of rows with boom up. In this section, we use x to denote easting and y to denote northing.

Figure 9 compares different methods for reconstructing the northing trajectory. The P-spline reconstruction fails due to instances where $y_{i+1} = y_i$. Wavelet (*sure*) overshoots at turning points, as does the non-adaptive V-spline, though more smoothly. The non-adaptive V-spline overshoots because it is incorporating outdated velocity information during a period where the velocity is changing quickly. On the other hand, wavelet (*BayesThresh*), the adaptive V-spline with $\gamma = 0$ and the adaptive V-spline give acceptable results.

5.3 2-Dimensional Trajectory

Figure 10 shows the full 2D adaptive V-spline reconstruction of the tractor trajectory for the first 512 observations, as well as the derived northing and easting trajectories. Also depicted by red dots of varying sizes are the sizes of the penalty terms λ_i . As expected, the penalty terms typically become large at turning points and before long waiting periods. A histogram of the λ_i and the implied penalty function $\lambda(t)$ are given in Figure 11. Figure 12 is a full reconstruction from the complete dataset.

6 Discussion

In this paper, a smoothing spline called the V-spline is proposed that minimizes an objective function which incorporates both position and velocity information. Given n knots, the V-spline has $2n$ degrees of freedom corresponding to $n - 1$ cubic polynomials with their value and first derivative matched at the $n - 2$ interior knots. The degrees of freedom are then fixed by n position observations and n velocity observations. Note that in the limit $\gamma \rightarrow 0$, the V-spline reduces to having n degrees of freedom. (See Appendix C for details.) An adaptive version of the V-spline is also introduced that seeks to control the impact of irregularly sampled observations and noisy velocity measurements. In simulation studies, the V-spline shows improved true mean squared error in reconstructions.

In most work on polynomial smoothing splines, observation errors are assumed to be independent. However, this can be a questionable assumption in practice and it is known that correlation greatly affects the selection of smoothing parameters (Wang, 1998). Parameter selection methods such as generalized maximum likelihood (GML), generalized cross-validation (GCV) typically underestimate smoothing parameters when data are correlated. To accommodate an autocorrelated error sequence, Diggle and Hutchinson (1989) extend GCV, and Wang (1998) extends GML and unbiased risk (UBR) to simultaneously estimate the smoothing and correlation parameters. Kohn et al. (1992) also propose an algorithm to evaluate cross-validation functions when the autocorrelated errors are modelled by an autoregressive moving average. Here we show that there is a generalized cross-validation scheme for the V-spline that is appropriate for correlated observation errors.

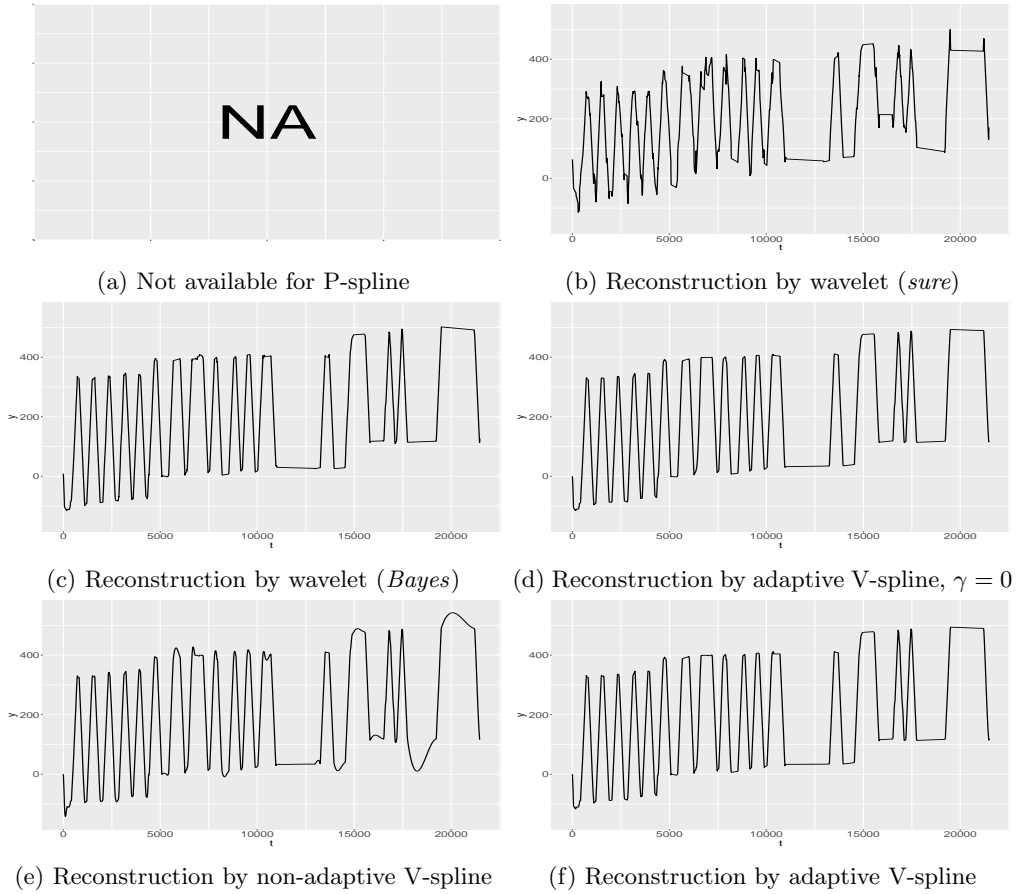
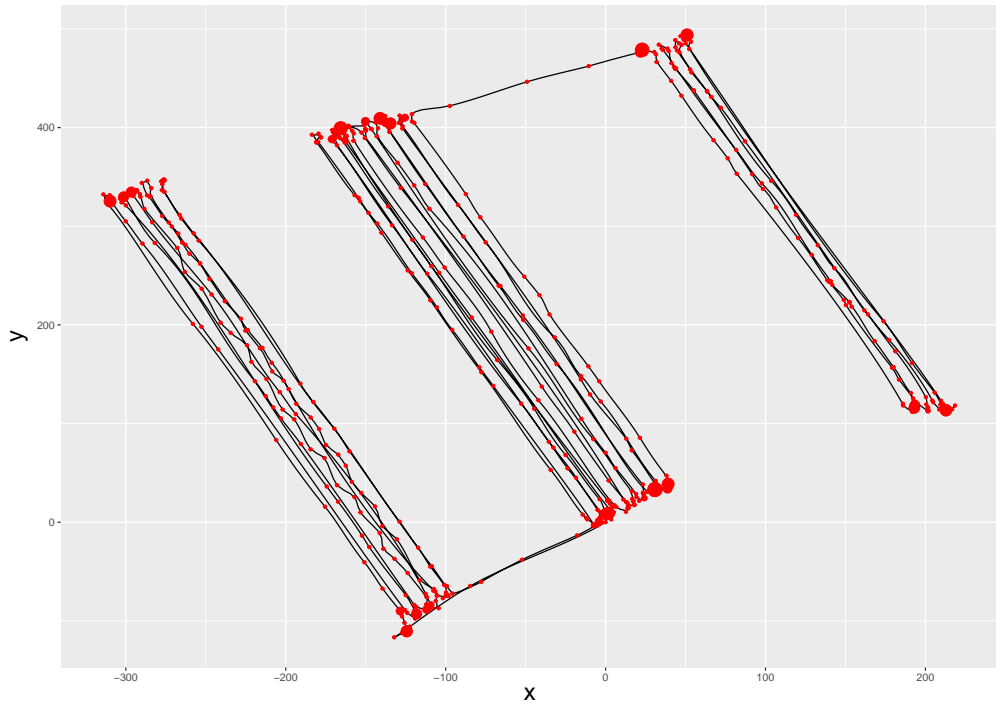
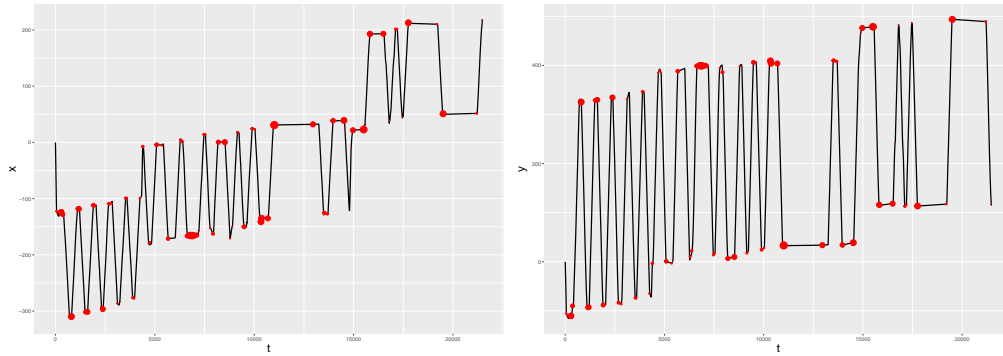


Figure 9: Fitted northing trajectories. Figure 9a The P-spline fails due to instances where $y_{i+1} = y_i$, which lead to issues with invertibility. Figure 9b Wavelet (*sure*) exhibiting overshooting at turning points. Figure 9c Wavelet (*BayesThresh*) showing improvement over wavelet (*sure*). Figure 9d The adaptive V-spline that does not incorporate velocity information. Figure 9e Non-adaptive V-spline exhibiting smooth overshooting at turning points. Figure 9f The adaptive V-spline that includes velocity information.



(a) Reconstruction of northing y vs easting x



(b) Derived easting x and northing y trajectories vs time t

Figure 10: Full 2-dimensional reconstruction; larger red dots indicate larger values of λ_i .

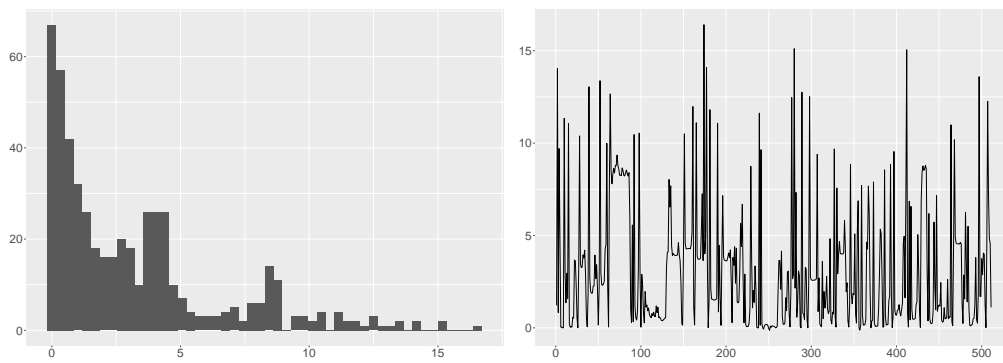


Figure 11: Histogram of the λ_i and implied penalty function $\lambda(t)$

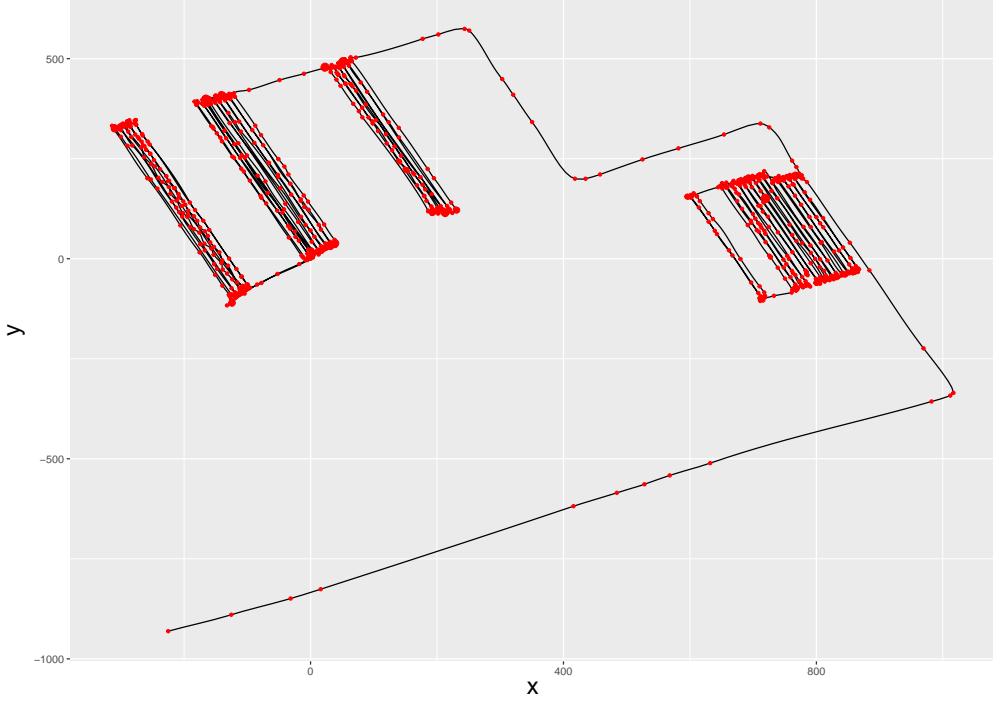


Figure 12: Full 2-dimensional reconstruction for the complete dataset; larger red dots indicate larger values of λ_i .

When observation errors are correlated (and considering splines in one-dimension for simplicity), the V-spline minimizes

$$\frac{1}{n} (\mathbf{y} - \mathbf{f})^\top W_1 (\mathbf{y} - \mathbf{f}) + \frac{\gamma}{n} (\mathbf{v} - \mathbf{f}')^\top W_2 (\mathbf{v} - \mathbf{f}') + \sum_{i=1}^{n-1} \lambda_i \int_{t_i}^{t_{i+1}} (f''(t))^2 dt, \quad (33)$$

where W_1 and W_2 are precision matrices, assumed known. The solution is $\hat{f}(t) = \sum_{k=1}^{2n} N_k(t) \hat{\theta}_k$, where

$$\hat{\theta} = (B^\top W_1 B + \gamma C^\top W_2 C + n\Omega_\lambda)^{-1} (B^\top W_1 \mathbf{y} + \gamma C^\top W_2 \mathbf{v}). \quad (34)$$

The usual leave-one-out cross-validation algorithm requires knowledge of the diagonal elements of the smoother matrices. GCV achieves computational savings and robustness by approximating $S_{ii} \approx \frac{1}{n} \text{tr}(S)$, etc. (Syed, 2011). The natural extension of the GCV to the V-spline with correlated errors is

$$\text{GCV}(\lambda, \gamma) = \frac{(\hat{\mathbf{f}} - \mathbf{y})^\top W_1 (\hat{\mathbf{f}} - \mathbf{y}) + \frac{2\text{tr}(\gamma T)}{\text{tr}(I - \gamma V)} (\hat{\mathbf{f}} - \mathbf{y})^\top W_1^{1/2} (W_2^{1/2})^\top (\hat{\mathbf{f}}' - \mathbf{v}) + \left(\frac{\text{tr}(\gamma T)}{\text{tr}(I - \gamma V)} \right)^2 (\hat{\mathbf{f}}' - \mathbf{v})^\top W_2 (\hat{\mathbf{f}}' - \mathbf{v})}{\left(\text{tr} \left(I - S - \frac{\text{tr}(\gamma T)}{\text{tr}(I - \gamma V)} U \right) \right)^2} \quad (35)$$

One current drawback of the V-spline is that it is slower than other spline-based methods, however we have not yet optimized CV parameter estimation, particularly around solving for $\hat{\theta}$ in (15). Future directions for the V-spline include application to ship tracking (Hintzen et al., 2010) and development of a fast on-line filtering mode.

Acknowledgements

This work was funded by grant UOOX1208 from the Ministry of Business, Innovation & Employment (NZ). GPS data was provided by TracMap (NZ).

A Penalty Matrix in (12)

We have $\Omega_\lambda = \sum_{i=1}^{n-1} \lambda_i \Omega^{(i)}$, where $[\Omega^{(i)}]_{jk} = \int_{t_i}^{t_{i+1}} N_j''(t) N_k''(t) dt$. Thus $\Omega^{(i)}$ is a $2n \times 2n$ bandwidth four symmetric matrix and its non-zero, upper triangular elements are

$$\Omega_{2i-1, 2i-1}^{(i)} = \int_{t_i}^{t_{i+1}} \frac{d^2 h_{00}^{(i)}(t)}{dt^2} \frac{d^2 h_{00}^{(i)}(t)}{dt^2} dt = \frac{12}{\Delta T_i^3} \quad (36)$$

$$\Omega_{2i-1, 2i}^{(i)} = \int_{t_i}^{t_{i+1}} \frac{d^2 h_{00}^{(i)}(t)}{dt^2} \frac{d^2 h_{10}^{(i)}(t)}{dt^2} dt = \frac{6}{\Delta T_i^2} \quad (37)$$

$$\Omega_{2i-1, 2i+1}^{(i)} = \int_{t_i}^{t_{i+1}} \frac{d^2 h_{00}^{(i)}(t)}{dt^2} \frac{d^2 h_{01}^{(i)}(t)}{dt^2} dt = \frac{-12}{\Delta T_i^3} \quad (38)$$

$$\Omega_{2i-1, 2i+2}^{(i)} = \int_{t_i}^{t_{i+1}} \frac{d^2 h_{00}^{(i)}(t)}{dt^2} \frac{d^2 h_{11}^{(i)}(t)}{dt^2} dt = \frac{6}{\Delta T_i^2} \quad (39)$$

$$\Omega_{2i, 2i}^{(i)} = \int_{t_i}^{t_{i+1}} \frac{d^2 h_{10}^{(i)}(t)}{dt^2} \frac{d^2 h_{10}^{(i)}(t)}{dt^2} dt = \frac{4}{\Delta T_i} \quad (40)$$

$$\Omega_{2i, 2i+1}^{(i)} = \int_{t_i}^{t_{i+1}} \frac{d^2 h_{10}^{(i)}(t)}{dt^2} \frac{d^2 h_{01}^{(i)}(t)}{dt^2} dt = \frac{-6}{\Delta T_i^2} \quad (41)$$

$$\Omega_{2i, 2i+2}^{(i)} = \int_{t_i}^{t_{i+1}} \frac{d^2 h_{10}^{(i)}(t)}{dt^2} \frac{d^2 h_{11}^{(i)}(t)}{dt^2} dt = \frac{2}{\Delta T_i} \quad (42)$$

$$\Omega_{2i+1, 2i+1}^{(i)} = \int_{t_i}^{t_{i+1}} \frac{d^2 h_{01}^{(i)}(t)}{dt^2} \frac{d^2 h_{01}^{(i)}(t)}{dt^2} dt = \frac{12}{\Delta T_i^3} \quad (43)$$

$$\Omega_{2i+1, 2i+2}^{(i)} = \int_{t_i}^{t_{i+1}} \frac{d^2 h_{01}^{(i)}(t)}{dt^2} \frac{d^2 h_{11}^{(i)}(t)}{dt^2} dt = \frac{-6}{\Delta T_i^2} \quad (44)$$

$$\Omega_{2i+2, 2i+2}^{(i)} = \int_{t_i}^{t_{i+1}} \frac{d^2 h_{11}^{(i)}(t)}{dt^2} \frac{d^2 h_{11}^{(i)}(t)}{dt^2} dt = \frac{4}{\Delta T_i} \quad (45)$$

where $\Delta T_i = t_{i+1} - t_i$ and $i = 1, 2, \dots, n-1$.

B Proof of Theorem 1

Our proof is an extension of the smoothing spline proof in Green and Silverman (1993).

Proof. If $g : [a, b] \rightarrow \mathbb{R}$ is a proposed minimizer, construct a cubic spline $f(t)$ that agrees with $g(t)$ and its first derivatives at t_1, \dots, t_n , and is linear on $[a, t_1]$ and $[t_n, b]$. Let $h(t) = g(t) - f(t)$. Then, for $i = 1, \dots, n-1$,

$$\begin{aligned} \int_{t_i}^{t_{i+1}} f''(t) h''(t) dt &= f''(t) h'(t) \Big|_{t_i}^{t_{i+1}} - \int_{t_i}^{t_{i+1}} f'''(t) h'(t) dt \\ &= 0 - f'''(t_i^+) \int_{t_i}^{t_{i+1}} h'(t) dt \\ &= -f'''(t_i^+) (h(t_{i+1}) - h(t_i)) = 0. \end{aligned}$$

Additionally, $\int_a^{t_1} f''(t) h''(t) dt = \int_{t_n}^b f''(t) h''(t) dt = 0$, since $f(t)$ is assumed linear outside the

knots. Thus, for $i = 0, \dots, n$,

$$\begin{aligned}
\int_{t_i}^{t_{i+1}} |g''(t)|^2 dt &= \int_{t_i}^{t_{i+1}} |f''(t) + h''(t)|^2 dt \\
&= \int_{t_i}^{t_{i+1}} |f''(t)|^2 dt + 2 \int_{t_i}^{t_{i+1}} f''(t)h''(t) dt + \int_{t_i}^{t_{i+1}} |h''(t)|^2 dt \\
&= \int_{t_i}^{t_{i+1}} |f''(t)|^2 dt + \int_{t_i}^{t_{i+1}} |h''(t)|^2 dt \\
&\geq \int_{t_i}^{t_{i+1}} |f''(t)|^2 dt.
\end{aligned}$$

The result $J[f] \leq J[g]$ follows since $\lambda_i > 0$.

Furthermore, equality of the curvature penalty term only holds if $g(t) = f(t)$. On $[t_1, t_n]$, we require $h''(t) = 0$ but since $h(t_i) = h'(t_i) = 0$ for $i = 1, \dots, n$, this means $h(t) = 0$. Meanwhile on $[a, t_1]$ and $[t_n, b]$, $f''(t) = 0$ so that equality requires $g''(t) = 0$. Since $f(t)$ agrees with $g(t)$ and its first derivatives at t_1 and t_n , equality is forced on both intervals. \square

C Proof of Theorem 2

Proof. Let $Q_\lambda = C\Omega_\lambda = C \sum_{i=1}^{n-1} \lambda_i \Omega^{(i)}$, which is simply the even rows of Ω_λ . Multiplying both sides of (15) by CG , where $G = B^\top B + \gamma C^\top C + n\Omega_\lambda$, and using the fact that $CB^\top = 0$ and $CC^\top = I$, we find

$$Q_\lambda \hat{\theta} = \frac{\gamma}{n} (\mathbf{v} - \mathbf{f}').$$

We note in passing that when $\gamma = 0$, $Q_\lambda \hat{\theta} = 0$. Since Q_λ is an $n \times 2n$ matrix of full rank (this can be established from results below), the degrees of freedom of the V-spline decrease from $2n$ to n when the velocity information is removed, as one would expect.

The only basis functions with support on $[t_i, t_{i+1})$ are the $N_k(t)$ with $k \in \{2i - 1, 2i, 2i + 1, 2i + 2\}$. Integrating by parts and using properties of the basis functions at the knots, we obtain the non-zero elements of the even rows of $\Omega^{(i)}$:

$$\Omega_{2i,k}^{(i)} = -N_k''(t_i^+), \quad \Omega_{2i+2,k}^{(i)} = N_k''(t_{i+1}^-),$$

where $k \in \{2i - 1, 2i, 2i + 1, 2i + 2\}$. The actual numerical values are given in Appendix A and confirm that Q_λ has full rank. It follows that

$$(Q_\lambda \hat{\theta})_i = \left(\lambda_{i-1} \Omega_{2i,\cdot}^{(i-1)} + \lambda_i \Omega_{2i,\cdot}^{(i)} \right) \hat{\theta} = \lambda_{i-1} f''(t_i^-) - \lambda_i f''(t_i^+),$$

where it is understood that $f''(t_1^-) = f''(t_n^+) = 0$. Thus the backward implication is clear.

Continuity of $f''(t)$ at $t = t_1$ implies $\gamma(v_1 - f'_1) = 0$. If we can show $\gamma = 0$, then continuity of $f''(t)$ at the remaining observation times will establish the forward implication. Suppose instead $v_1 = f'_1$. Then from (15), we have $v_1 = (0 \ 1 \ 0 \ \dots \ 0) G^{-1} (B^\top \mathbf{y} + \gamma C^\top \mathbf{v})$. For almost all \mathbf{y} and \mathbf{v} , this implies $(0 \ 1 \ 0 \ \dots \ 0)^\top$ is an eigenvector of G with eigenvalue γ . But, using the numerical values from Appendix A, the second column of G is $(\frac{6\lambda_1}{\Delta T^2} \ \gamma + \frac{4\lambda_1}{\Delta T} \ \frac{-6\lambda_1}{\Delta T^2} \ \frac{2\lambda_1}{\Delta T} \ 0 \ \dots \ 0)^\top \neq \gamma(0 \ 1 \ 0 \ \dots \ 0)^\top$, since $\lambda_1 > 0$. \square

D Proof of Theorem 3

Proof. We start with the following lemma:

Lemma 4. For $\lambda(t)$, γ and for fixed i , let $\mathbf{f}^{(-i)}$ be the vector with components $f_j^{(-i)} = \hat{f}^{(-i)}(t_j, \lambda, \gamma)$, $\mathbf{f}'^{(-i)}$ by the vector with components $f_j'^{(-i)} = \hat{f}'^{(-i)}(t_j, \lambda, \gamma)$, and define vectors \mathbf{y}^* and \mathbf{v}^* by

$$\begin{cases} y_j^* = y_j & j \neq i \\ y_i^* = \hat{f}^{(-i)}(t_i) & \text{otherwise} \end{cases} \quad (46)$$

$$\begin{cases} v_j^* = v_j & j \neq i \\ v_i^* = \hat{f}'^{(-i)}(t_i) & \text{otherwise} \end{cases} \quad (47)$$

Then

$$\hat{\mathbf{f}}^{(-i)} = S\mathbf{y}^* + \gamma T\mathbf{v}^* \quad (48)$$

$$\hat{\mathbf{f}}'^{(-i)} = U\mathbf{y}^* + \gamma V\mathbf{v}^* \quad (49)$$

Proof. For any smooth curve f with \mathbf{y}^* and \mathbf{v}^* , we have

$$\begin{aligned} & \frac{1}{n} \sum_{j=1}^n (y_j^* - f(t_j))^2 + \frac{\gamma}{n} \sum_{j=1}^n (v_j^* - f'(t_j))^2 + \sum_{j=1}^n \lambda_j \int_{t_j}^{t_{j+1}} (f''(t))^2 dt \\ & \geq \frac{1}{n} \sum_{j \neq i} (y_j^* - f(t_j))^2 + \frac{\gamma}{n} \sum_{j \neq i} (v_j^* - f'(t_j))^2 + \sum_{j=1}^n \lambda_j \int_{t_j}^{t_{j+1}} (f''(t))^2 dt \\ & \geq \frac{1}{n} \sum_{j \neq i} (y_j^* - \hat{f}^{(-i)}(t_j))^2 + \frac{\gamma}{n} \sum_{j \neq i} (v_j^* - \hat{f}'^{(-i)}(t_j))^2 + \sum_{j=1}^n \lambda_j \int_{t_j}^{t_{j+1}} (\hat{f}''^{(-i)}(t))^2 dt \\ & = \frac{1}{n} \sum_{j=1}^n (y_j^* - \hat{f}^{(-i)}(t_j))^2 + \frac{\gamma}{n} \sum_{j=1}^n (v_j^* - \hat{f}'^{(-i)}(t_j))^2 + \sum_{j=1}^n \lambda_j \int_{t_j}^{t_{j+1}} (\hat{f}''^{(-i)}(t))^2 dt \end{aligned}$$

by the definition of $\hat{\mathbf{f}}^{(-i)}$, $\hat{\mathbf{f}}'^{(-i)}$ and the fact that $y_i^* = \hat{f}^{(-i)}(t_i)$, $v_i^* = \hat{f}'^{(-i)}(t_i)$. It follows that $\hat{f}^{(-i)}$ is the minimizer of the objective function (4), so that

$$\hat{\mathbf{f}}^{(-i)} = S\mathbf{y}^* + \gamma T\mathbf{v}^*$$

$$\hat{\mathbf{f}}'^{(-i)} = U\mathbf{y}^* + \gamma V\mathbf{v}^*$$

as required. \square

As a consequence of lemma 4, we obtain expressions for the deleted residuals $y_i - \hat{f}^{(-i)}(t_i)$ and $v_i - \hat{f}'^{(-i)}(t_i)$ in terms of $y_i - \hat{f}(t_i)$ and $v_i - \hat{f}'(t_i)$ respectively:

$$\begin{aligned} \hat{f}^{(-i)}(t_i) - y_i &= \sum_{j=1}^n S_{ij} y_j^* + \gamma \sum_{j=1}^n T_{ij} v_j^* - y_i^* \\ &= \sum_{j \neq i}^n S_{ij} y_j + \gamma \sum_{j \neq i}^n T_{ij} v_j + S_{ii} \hat{f}^{(-i)}(t_i) + \gamma T_{ii} \hat{f}'^{(-i)}(t_i) - y_i \\ &= \sum_{j=1}^n S_{ij} y_j + \gamma \sum_{j=1}^n T_{ij} v_j + S_{ii} (\hat{f}^{(-i)}(t_i) - y_i) + \gamma T_{ii} (\hat{f}'^{(-i)}(t_i) - v_i) - y_i \\ &= (\hat{f}(t_i) - y_i) + S_{ii} (\hat{f}^{(-i)}(t_i) - y_i) + \gamma T_{ii} (\hat{f}'^{(-i)}(t_i) - v_i) \end{aligned} \quad (50)$$

and

$$\begin{aligned}
\hat{f}'^{(-i)}(t_i) - v_i &= \sum_{j=1}^n U_{ij} y_j^* + \gamma \sum_{j=1}^n V_{ij} v_j^* - v_i^* \\
&= \sum_{j \neq i}^n U_{ij} y_j + \gamma \sum_{j \neq i}^n V_{ij} v_j + U_{ii} \hat{f}^{(-i)}(t_i) + \gamma V_{ii} \hat{f}'^{(-i)}(t_i) - v_i \\
&= \sum_{j=1}^n U_{ij} y_j + \gamma \sum_{j=1}^n V_{ij} v_j + U_{ii} \left(\hat{f}^{(-i)}(t_i) - y_i \right) + \gamma V_{ii} \left(\hat{f}'^{(-i)}(t_i) - v_i \right) - v_i \\
&= \left(\hat{f}'(t_i) - v_i \right) + U_{ii} \left(\hat{f}^{(-i)}(t_i) - y_i \right) + \gamma V_{ii} \left(\hat{f}'^{(-i)}(t_i) - v_i \right).
\end{aligned} \tag{51}$$

Thus

$$\hat{f}'^{(-i)}(t_i) - v_i = \frac{\hat{f}'(t_i) - v_i}{1 - \gamma V_{ii}} + \frac{U_{ii} \left(\hat{f}^{(-i)}(t_i) - y_i \right)}{1 - \gamma V_{ii}}. \tag{52}$$

By substituting equation (52) into (50), we obtain

$$\hat{f}^{(-i)}(t_i) - y_i = \frac{\hat{f}(t_i) - y_i + \gamma \frac{T_{ii}}{1 - \gamma V_{ii}} \left(\hat{f}'(t_i) - v_i \right)}{1 - S_{ii} - \gamma \frac{T_{ii}}{1 - \gamma V_{ii}} U_{ii}}.$$

Consequently,

$$CV(\lambda, \gamma) = \frac{1}{n} \sum_{i=1}^n \left(\frac{\hat{f}(t_i) - y_i + \gamma \frac{T_{ii}}{1 - \gamma V_{ii}} \left(\hat{f}'(t_i) - v_i \right)}{1 - S_{ii} - \gamma \frac{T_{ii}}{1 - \gamma V_{ii}} U_{ii}} \right)^2.$$

□

References

- Abramovich, F., Sapatinas, T., and Silverman, B. W. (1998). Wavelet thresholding via a Bayesian approach. *Journal of the Royal Statistical Society: Series B (Statistical Methodology)*, 60(4):725–749.
- Agarwal, P. K., Arge, L., and Erickson, J. (2003). Indexing moving points. *Journal of Computer and System Sciences*, 66(1):207–243.
- Aydin, D. and Tuzemen, M. S. (2012). Smoothing parameter selection problem in nonparametric regression based on smoothing spline: A simulation study. *Journal of Applied Sciences*, 12(7):636.
- Ben-Arieh, D., Chang, S., Rys, M., and Zhang, G. (2004). Geometric modeling of highways using global positioning system data and B-spline approximation. *Journal of Transportation Engineering*, 130(5):632–636.
- Castro, M., Iglesias, L., Rodríguez-Solano, R., and Sánchez, J. A. (2006). Geometric modelling of highways using global positioning system (GPS) data and spline approximation. *Transportation Research Part C: Emerging Technologies*, 14(4):233–243.
- Craven, P. and Wahba, G. (1978). Smoothing noisy data with spline functions. *Numerische Mathematik*, 31(4):377–403.
- Diggle, P. J. and Hutchinson, M. F. (1989). On spline smoothing with autocorrelated errors. *Australian & New Zealand Journal of Statistics*, 31(1):166–182.
- Donoho, D. L. and Johnstone, I. M. (1995). Adapting to unknown smoothness via wavelet shrinkage. *Journal of the American Statistical Association*, 90(432):1200–1224.

- Donoho, D. L., Johnstone, I. M., Kerkyacharian, G., and Picard, D. (1995). Wavelet shrinkage: asymptopia? *Journal of the Royal Statistical Society. Series B (Methodological)*, 57(2):301–369.
- Donoho, D. L. and Johnstone, J. M. (1994). Ideal spatial adaptation by wavelet shrinkage. *Biometrika*, 81(3):425–455.
- Dubins, L. E. (1957). On curves of minimal length with a constraint on average curvature, and with prescribed initial and terminal positions and tangents. *American Journal of Mathematics*, 79(3):497–516.
- Erkorkmaz, K. and Altintas, Y. (2001). High speed CNC system design. Part I: Jerk limited trajectory generation and quintic spline interpolation. *International Journal of Machine Tools and Manufacture*, 41(9):1323–1345.
- Gasparetto, A. and Zanotto, V. (2007). A new method for smooth trajectory planning of robot manipulators. *Mechanism and Machine Theory*, 42(4):455–471.
- Gloderer, M. and Hertle, A. (2010). Spline-based trajectory optimization for autonomous vehicles with Ackerman drive. Preprint available at <http://ais.informatik.uni-freiburg.de/teaching/ws09/robotics2/projects/mr2-p6-paper.pdf>.
- Green, P. J. and Silverman, B. W. (1993). *Nonparametric regression and generalized linear models: a roughness penalty approach*. CRC Press.
- Gu, C. (1998). Model indexing and smoothing parameter selection in nonparametric function estimation. *Statistica Sinica*, 8(3):607–623.
- Hastie, T., Tibshirani, R., and Friedman, J. H. (2009). *The Elements of Statistical Learning: Data Mining, Inference, and Prediction. Second Edition*. Springer-Verlag.
- Hintzen, N. T., Piet, G. J., and Brunel, T. (2010). Improved estimation of trawling tracks using cubic Hermite spline interpolation of position registration data. *Fisheries Research*, 101(1):108–115.
- Kohn, R., Ansley, C. F., and Wong, C.-M. (1992). Nonparametric spline regression with autoregressive moving average errors. *Biometrika*, 79(2):335–346.
- Komoriya, K. and Tanie, K. (1989). Trajectory design and control of a wheel-type mobile robot using B-spline curve. In *Intelligent Robots and Systems' 89. The Autonomous Mobile Robots and Its Applications. IROS'89. Proceedings., IEEE/RSJ International Workshop*, pages 398–405. IEEE.
- Krivobokova, T., Crainiceanu, C. M., and Kauermann, G. (2008). Fast adaptive penalized splines. *Journal of Computational and Graphical Statistics*, 17(1):1–20.
- Liu, Z. and Guo, W. (2010). Data driven adaptive spline smoothing. *Statistica Sinica*, 20(3):1143–1163.
- Magid, E., Keren, D., Rivlin, E., and Yavneh, I. (2006). Spline-based robot navigation. In *Intelligent Robots and Systems, 2006 IEEE/RSJ International Conference*, pages 2296–2301. IEEE.
- Nason, G. (2010). *Wavelet methods in statistics with R*. Springer Science & Business Media.
- Ruppert, D., Wand, M. P., and Carroll, R. J. (2003). *Semiparametric Regression*. Cambridge University Press.
- Schwarz, K.-P. (2000). *Geodesy Beyond 2000: The Challenges of the First Decade, IAG General Assembly Birmingham, July 19–30, 1999*. Springer Science & Business Media.
- Sealfon, C., Verde, L., and Jimenez, R. (2005). Smoothing spline primordial power spectrum reconstruction. *Physical Review D*, 72(10):103520.

- Silverman, B. W. (1985). Some aspects of the spline smoothing approach to non-parametric regression curve fitting. *Journal of the Royal Statistical Society. Series B (Methodological)*, 47(1):1–52.
- Syed, A. R. (2011). A review of cross validation and adaptive model selection. Master’s thesis, Georgia State University, Atlanta, GA.
- Wahba, G. (1985). A comparison of GCV and GML for choosing the smoothing parameter in the generalized spline smoothing problem. *The Annals of Statistics*, 13(4):1378–1402.
- Wang, X., Jiang, P., Li, D., and Sun, T. (2017). Curvature continuous and bounded path planning for fixed-wing UAVs. *Sensors*, 17(9):2155.
- Wang, Y. (1998). Smoothing spline models with correlated random errors. *Journal of the American Statistical Association*, 93(441):341–348.
- Yang, K. and Sukkarieh, S. (2010). An analytical continuous-curvature path-smoothing algorithm. *Robotics, IEEE Transactions on*, 26(3):561–568.
- Yao, F., Müller, H.-G., Wang, J.-L., et al. (2005). Functional linear regression analysis for longitudinal data. *The Annals of Statistics*, 33(6):2873–2903.
- Yu, B., Kim, S. H., Bailey, T., and Gamboa, R. (2004). Curve-based representation of moving object trajectories. In *Database Engineering and Applications Symposium, 2004. IDEAS’04. Proceedings. International*, pages 419–425. IEEE.
- Zhang, K., Guo, J.-X., and Gao, X.-S. (2013). Cubic spline trajectory generation with axis jerk and tracking error constraints. *International Journal of Precision Engineering and Manufacturing*, 14(7):1141–1146.